PCCP

Accepted Manuscript

This is an *Accepted Manuscript*, which has been through the Royal Society of Chemistry peer review process and has been accepted for publication.

Accepted Manuscripts are published online shortly after acceptance, before technical editing, formatting and proof reading. Using this free service, authors can make their results available to the community, in citable form, before we publish the edited article. We will replace this *Accepted Manuscript* with the edited and formatted *Advance Article* as soon as it is available.

You can find more information about *Accepted Manuscripts* in the Information for Authors.

Please note that technical editing may introduce minor changes to the text and/or graphics, which may alter content. The journal's standard Terms & Conditions and the Ethical guidelines still apply. In no event shall the Royal Society of Chemistry be held responsible for any errors or omissions in this *Accepted Manuscript* or any consequences arising from the use of any information it contains.

ROYAL SOCIETY OF CHEMISTRY

www.rsc.org/pccp

Highly Efficient $(In_2Te_3)_x(GeTe)_{3-3x}$ Thermoelectric Materials: A Substitute for TAGS

Hui Sun,[1†] Xu Lu,[2†] Hang Chi[1], Donald T. Morelli,[2] and Ctirad Uher[1]*

[1]*Department of Physics, University of Michigan, Ann Arbor, Michigan 48109, USA*

[2]*Department of Chemical Engineering and Materials Science, Michigan State University, East Lansing, Michigan 48824, USA*

* To whom correspondence should be addressed. cuher@umich.edu

† These authors contributed equally to this work.

Abstract

GeTe is a versatile base compound to produce highly efficient p-type thermoelectric materials such as the TAGS materials $(AgSbTe_2)_{1-x}(GeTe)_x$ and GeTe-PbTe nanocomposites. The pure GeTe composition shows a very high power factor, ~ 42 $\mu Wcm^{-1}K^{-2}$, between 673 K and 823 K, which is among the highest power factors that have ever been reported in this temperature range. However, its relatively high thermal conductivity limits the dimensionless figure of merit *ZT* to values of only unity. In this paper, we present an efficient approach to reduce the thermal conductivity by preparing $(In_2Te_3)_x(GeTe)_{3-3x}$ solid solutions. In spite of a slight degradation of the electronic properties, the drastic reduction of the thermal conductivity due to a synergistic combination of reduced electronic thermal conductivity, strong alloy scattering, and vacancy phonon scattering leads to *ZT* values as high as 1.35 at 823K for the x = 0.05 sample. Our results show that $(In_2Te_3)_x(GeTe)_{3-3x}$ is a prospective substitute for TAGS as a p-leg element for high-temperature power generation.

Physical Chemistry Chemical Physics Accepted Manuscript

Introduction

Attributed to its capability to achieve the direct conversion between heat energy and electricity, thermoelectricity has becomes an appealing energy conversion technique in recent decades. Devices composed of thermoelectric (TE) materials can either act as a generator to produce electric power from waste heat or solar radiation, or function as a solid-state refrigerator to realize spot cooling of electronic devices or provide individual climate control in automobiles[1]. Applications of TE devices mainly depend on the material's TE efficiency. This is evaluated by the dimensionless figure of merit[2] $ZT=S^2T/\rho\kappa$, where S is the Seebeck coefficient, T is the absolute temperature, ρ is the electrical resistivity and κ is the thermal conductivity. Therefore, highly efficient TE materials should possess a large power factor (S^2/ρ) but low thermal conductivity.

Compounds belonging to the IV-VI family of semiconductors such as PbTe, SnTe, and GeTe attract continuous research interest in the TE field because their unique highly degenerate electronic structures give rise to quite large power factors at high temperature[3-8]. The pristine GeTe composition is self-doped by Ge vacancies and always presents p-type transport behavior[9]. It crystallizes in a rhombohedral structure ($R3m$) at room temperature and transforms to the NaCl-type cubic structure ($Fm\bar{3}m$) at ~ 670 K[10]. The phase transition is accompanied by an increase in the valence band degeneracy, and thus the power factor is maintained at quite large values at high temperature[7]. Exceptional electronic properties of GeTe have been recently reported by Levin et al. In their work[6], power factors as high as 42 $\mu Wcm^{-1}K^{-2}$ were obtained above 700 K, but the ZT was not better than unity due to the high thermal conductivity. When GeTe is combined with $AgSbTe_2$ to form a solid solution $(AgSbTe_2)_{100-x}(GeTe)_x$ (acronym TAGS-x, where x is the mole fraction of GeTe), an ultra low thermal conductivity can be obtained at x = 80 and 85, leading to quite a high ZT of 1.4 at ~700 K[11-13]. It is believed that the dramatic reduction of the thermal conductivity in TAGS materials is associated with either strong lattice strains or attributed to the twining boundaries and nano domains in the microstructure[11, 13]. Structural modifications through the phase transition of $Sb_2Te_3(GeTe)_n$ (n = 3-19) have been

Physical Chemistry Chemical Physics Accepted Manuscript

reported.[14] Moreover, the influence of phase transitions on thermoelectric properties has been studied in the $(GeTe)_nSbInTe_3$ ($n \leqslant 3$) compounds.[15] Various structure modifications of GeTe have been investigated very recently, several of which achieved impressive thermoelectric performance.[16-19]

In our work, we present the TE properties of another simple GeTe-based solid solutions, namely $(In_2Te_3)_x(GeTe)_{3-3x}$. According to the GeTe - In_2Te_3 pseudo binary phase diagram[20], the single phase solid solutions exist over a large In_2Te_3 concentration range, especially at high temperatures. The intentionally introduced alloying disorder and vacancies are expected not only to modify the electronic structures, but also to result in a huge reduction in the thermal conductivity[21]. We shall show that the excellent *ZT* at high temperatures makes these solid solutions a promising alternative for TAGS materials.

Experimental

Compositions of $(In_2Te_3)_x(GeTe)_{3-3x}$ with x = 0.00 – 0.20 were synthesized by melting the stoichiometric constituent elements in vacuum sealed quartz ampoules. The elements were first heated to 1273 K at a rate of 2 K/min and reacted for 8 hours, then slowly cooled at the same rate to 873 K and soaked for 24 hours. After furnace cooling to room temperature, ingots with a metallic luster were obtained. Ground ingots were then hot pressed at 773 K and 60 MPa for 30 min to form dense pucks. Powder x-ray diffraction (XRD) patterns were obtained using a Scintag X1 diffractometer with Cu $K\alpha$ radiation. Low-temperature (2 K - 300 K) electrical and thermal transport properties were simultaneously measured by a steady-state technique in a cryostat. Au/Fe-Chromel thermocouples were used to record the temperature and Cu wires acted as voltage probes. The high-temperature (300 K – 823 K) electrical properties were measured using an ULVAC ZEM-3 system and thermal conductivity was determined from $\kappa = D \times C_p \times d$, where D is the thermal diffusivity, C_p is the specific heat capacity and d is the sample density. The thermal diffusivity was obtained using the laser flash method with an Anter Flashline 5000 instrument. The data were also confirmed by a Netzsch LFA-457 laser flash system. The specific

Physical Chemistry Chemical Physics Accepted Manuscript

heat capacity was measured by differential scanning calorimetry (DSC) using a Netzsch DSC 404C apparatus. The sample densities measured by the Archimedes method were all above 96% of the corresponding x-ray density. Hall measurements were carried out in a Quantum Design MPMS system equipped with a Linear Research ac bridge (LR-700). The Hall carrier concentration and mobility were calculated using $p_H = 1/eR$ and $\mu_H = R/\rho$ respectively, where R is the Hall coefficient and e is the electron charge.

Results and Discussion

Figure 1(a) displays the XRD patterns for all samples investigated. The x = 0.00, 0.05 and 0.10 samples only show a single phase with the rhombohedral structure, while the x = 0.15 and 0.20 samples present a different crystal structure without noticeable impurity phases. A well-known character of the GeTe rhombohedral structure[22] is the occurrence of split (024) and (220) peaks at $41^o \leq 2\theta \leq 45^o$ as shown in the inset in Figure 1(a). During the phase transition at elevated temperature, the split peaks merge and a single (220) reflection for the cubic polymorph appears within this 2θ range[22]. For our samples, the (024) and (220) doublets shift towards one another with increasing x, and eventually form a single broad peak for x = 0.15 and 0.20, indicating a higher symmetry close to the cubic structure for these two samples at room temperature. This phenomenon is also observed in TAGS materials, where the split peaks get closer and the unit cell angle approaches 90^o with increasing $AgSbTe_2$ concentration[12, 13]. However, we cannot claim that the x = 0.15 and 0.20 samples crystallize in the cubic structure because the much broadened peak is very likely caused by an overlap of the doublets and the small reflection peaks at $2\theta \sim 25^o$ cannot be attributed to the cubic structure. This question can be clarified by the DSC measurements. As shown in Figure 1(b), a spike appears for all samples in their temperature-dependent specific heat capacity curves, suggesting that each sample experiences a phase transition[12]. The peak temperature for pure GeTe is 683 K, consistent with the previously reported phase transition temperature. Note that the peak temperature gradually decreases to ~508 K with the increasing In_2Te_3 concentration, a trend similar to that of the TAGS

Physical Chemistry Chemical Physics Accepted Manuscript

system[12]. Therefore, we conclude that the x = 0.15 and 0.20 samples possess only a pseudo cubic structure.

The temperature-dependent electrical transport results are shown in Figure 2. As can be seen in Figure 2(a), the electrical resistivity monotonically increases with the increasing In_2Te_3 content over the entire investigated temperature range. The phase transition phenomenon of each sample is also distinguishable from the resistivity-temperature curve. A knee appears in the resistivity curve for x = 0.00 and 0.05 while an abrupt drop of the resistivity is observed for the other three samples around the phase transition temperature determined by the DSC measurements. The Seebeck coefficient, as shown in Figure 2(b), is also increased by the rising In_2Te_3 concentration below 300 K, however, the change of the Seebeck coefficient is more complicated above room temperature. Based on the above results, one will naturally take into account a decrease in the carrier concentration with increasing x, particularly hole concentration since the Seebeck coefficient is positive, for the good mapping between the Seebeck coefficient and resistivity. However, the concentration of holes obtained from the Hall effect at 200 K, as presented in Table 1, approximately increases with increasing x and thus the rising resistivity is caused by the rapid reduction of the mobility as shown in Figure 3. This is in stark contrast to the aforementioned conjecture of a decrease in the hole concentration. As the magnitude of the Seebeck coefficient is determined by the position of the Fermi level relative to the band edge, the increasing hole concentration can be only understood by an enhanced hole effective mass or the density of states. A recent study on In-doped SnTe found a similar effect to ours in which an increase in the hole concentration was accompanied by a larger Seebeck coefficient[4]. The authors attributed the anomaly to the resonant levels in the valence band introduced by In doping. In our work, we suggest that a two parabolic valence band model can explain the enhanced effective mass equally well.

It is widely accepted that GeTe crystallizing in the rocksalt structure exhibits a band structure with a light valence band maximum (VBM) at the *L* point and a heavy second VBM along the Σ direction in the first Brillouin zone[23-25]. The low-temperature rhombohedral structure is formed

Physical Chemistry Chemical Physics Accepted Manuscript

through only a slight distortion of the cubic unit cell along the [111] direction and thus their electronic structures are considered roughly identical[25]. In the two-band model where acoustic phonon scattering is assumed dominant, each electronic transport coefficient can be calculated using the band parameters as follows[7]:

$$p_{\mathrm{l}} = 4\pi\left(\frac{2m_{\mathrm{l}}^{*}kT}{h^2}\right)^{3/2} F_{1/2}\left(\eta_{\mathrm{l}}\right)$$

$$p_{\mathrm{h}} = 4\pi\left(\frac{2m_{\mathrm{h}}^{*}kT}{h^2}\right)^{3/2} F_{1/2}\left(\eta_{\mathrm{h}}\right)$$

$$\Delta E = E_{\mathrm{l}} - E_{\mathrm{h}} = \left(\eta_{\mathrm{l}} - \eta_{\mathrm{h}}\right)\cdot kT$$

$$R = \frac{p_{\mathrm{h}} + p_{\mathrm{l}}\cdot b^2}{e\left(p_{\mathrm{h}} + p_{\mathrm{l}}\cdot b\right)^2}$$

$$S = \frac{p_{\mathrm{h}}}{p_{\mathrm{h}} + p_{\mathrm{l}}\cdot b}S_{\mathrm{h}} + \frac{p_{\mathrm{l}}\cdot b}{p_{\mathrm{h}} + p_{\mathrm{l}}\cdot b}S_{\mathrm{l}} \quad \text{and} \quad S_{\mathrm{h,l}} = \frac{k}{e}\left[\frac{2F_1\left(\eta_{\mathrm{h,l}}\right)}{F_0\left(\eta_{\mathrm{h,l}}\right)} - \eta_{\mathrm{h,l}}\right]$$

$$L = \frac{p_{\mathrm{h}}}{p_{\mathrm{h}} + p_{\mathrm{l}}\cdot b}L_{\mathrm{h}} + \frac{p_{\mathrm{l}}\cdot b}{p_{\mathrm{h}} + p_{\mathrm{l}}\cdot b}L_{\mathrm{l}} \quad \text{and} \quad L_{\mathrm{h,l}} = \left(\frac{k}{e}\right)^2\left\{\frac{3F_2\left(\eta_{\mathrm{h,l}}\right)}{F_0\left(\eta_{\mathrm{h,l}}\right)} - \left[\frac{2F_1\left(\eta_{\mathrm{h,l}}\right)}{F_0\left(\eta_{\mathrm{h,l}}\right)}\right]^2\right\}$$

$$F_r\left(\eta\right) = \int_0^{\infty}\frac{\varepsilon^r}{1+\exp(\varepsilon-\eta)}\mathrm{d}\varepsilon$$

where p is the hole concentration, m^* the density of states effective mass, k the Boltzmann constant, h the Planck constant, η the reduced chemical potential E/kT, $F_{\mathrm{r}}(\eta)$ the Fermi integral, ΔE the energy separation between the light and heavy VBM, b the mobility ratio of light hole to heavy hole, and L the Lorenz number. The subscripts h and l in all equations stand for heavy and light holes, respectively. The light band effective mass has been consistently reported as 0.5 m_0 where m_0 is the electron mass[7, 23]. Although Kolomoets et al.[7] took the heavy band effective mass as m_0, we find such a value too small to account for our data and the value of 2.5 m_0 better satisfies the transport results. The mobility ratio b is assumed as 4, the same value as that for SnTe and PbTe[3, 4]. Provided that the band effective masses and b are independent of the

Physical Chemistry Chemical Physics Accepted Manuscript

composition and doping only changes the chemical potentials and the band edge separation ΔE, we can obtain the temperature-dependent Seebeck coefficient (solid lines) and Hall coefficient (dashed lines) by fitting the experimental data, as presented in Figure 2(c). The fitting parameters and results for each sample are listed in Table 2. It is worth mentioning that the results for pristine GeTe in our calculation are comparable to the literature results, for example, ΔE = ~0.30 eV [7, 23] and $d\Delta E/dT = 3\times10^{-4}$ eV/K [24]. From Table 2, we can clearly see that the chemical potential continues to move toward the band edge and at the same time the energy separation decreases with the rising In_2Te_3 content. The heavy band becomes more populated and the density of states consequently gets enhanced. Another interesting feature is that the Seebeck coefficient increases more modestly for x = 0.10 and even eventually decreases for x = 0.15 and 0.20 at a certain temperature above 300 K, Figure 2(b). This behavior is in agreement with the upward shift of the chemical potential to the band edge and in this situation the bipolar effect can play a vital role in diminishing the Seebeck coefficient. In particular, the negative Hall coefficient for x = 0.20 at 250 K, Figure 2(c), reflects that electrons start to participate in the transport. The bipolar effect may also be evident in the increase of the thermal conductivity as we shall see later. Figure 2(d) depicts the power factor as a function of temperature for all studied samples. Our pure GeTe shows a very high power factor of 42 $\mu Wcm^{-1}K^{-2}$ at temperatures above 673 K, the same as the recently reported value for GeTe with a similar hole concentration[6]. The introduction of In_2Te_3 leads to a decrease in the power factor at high temperatures, however, the x = 0.05 sample still possesses a relatively high value of ~ 38 $\mu Wcm^{-1}K^{-2}$ between 623 K and 823 K. We note that this power factor is the highest among TE tellurides and TAGS materials within this temperature range.

The thermal conductivity for our samples is shown in Figure 4(a). In general, the total thermal conductivity is the sum of the electronic contribution (κ_e) and the lattice thermal conductivity (κ_L). The electronic part can be estimated using the Wiedemann-Franz law as $\kappa_e = LT/\rho$. The Lorenz number L is calculated using the high-temperature Seebeck coefficient data[26]. The calculated L is presented in the inset of Figure 4(b). We compared the near-room-temperature

Physical Chemistry Chemical Physics Accepted Manuscript

values here (Figure 4(b) inset) with the *L* values calculated from the two-band model (Table 2) and found that the difference is less than 7%. As one can see in Figure 4(a), the near-room-temperature thermal conductivity is continuously decreasing from 7.2 W/m K for x = 0.00 to 1.0 W/m K for x=0.20, due to the simultaneously reduced electronic and lattice thermal conductivity. However, the x = 0.10, 0.15 and 0.20 samples show rising thermal conductivity at elevated temperature as a consequence of the increased influence of the bipolar thermal conductivity contribution. Because the electronic part of the thermal conductivity, calculated via the Wiedemann-Franz law, does not account for the bipolar contribution to the thermal conductivity, the latter is also superposed on the lattice thermal conductivity in Figure 4(b). This phenomenon was also observed by a recent study in which one sample with the composition x = 0.20 (the same as our composition) was studied[27]. The apparent increase in the lattice part can be understood as arising from the bipolar effect. This observation is consistent with our discussion above concerning the trend of the Seebeck coefficient in these three samples. Regardless of the bipolar effect, the lattice thermal conductivity is decreased from 1.8 W/m K for x = 0.00 to 0.9 W/m K for x = 0.05 at 323 K and the latter sample shows lower lattice thermal conductivity than the pristine one over the entire temperature range. This reduction can be attributed to a strong phonon scattering by the mass and strain fluctuations between the vacancies/In and Ge host atoms[21].

The temperature-dependent *ZT* is displayed in Figure 5. The pristine GeTe itself exhibits a *ZT* of 1.0 at the highest temperatures due to its excellent electronic properties. The best *ZT* of 1.35 occurs in the x = 0.05 sample at 823 K and this sample also shows much higher average *ZT* than GeTe. Compared to the best performing TAGS materials[13], even though the x = 0.05 sample shows higher thermal conductivity, its larger power factor results in comparable *ZT* values and such a solid solution is a suitable substitute for TAGS as a p-type element.

All structural modifications of GeTe are accompanied by the development of particular nanostructures that can potentially influence transport behavior. The Seebeck coefficient is rather insensitive to the microstructure features provided no strong energy filtering takes place. The

Physical Chemistry Chemical Physics Accepted Manuscript

electrical conductivity is almost always adversely affected on account of enhanced charge carrier scattering. The real benefit of the presence of nanostructural features is the reduced thermal conductivity due to enhanced scattering of mid to long wavelength phonons. While some of these effects may potentially be at play in our materials, we strongly feel that the large compositional modifications that occur through alloying are the predominant drivers of property modification. The extent, if at all, to which specific nanostructural features influence the thermoelectric performance in GeTe-based compounds could be the focus of a future investigation of these materials.

Conclusion

The electrical and thermal transport properties of $(In_2Te_3)_x(GeTe)_{3-3x}$ materials from 2K to 823 K have been studied. Changes in the Hall coefficient and Seebeck coefficient with respect to the composition can be explained by a two valence band model. In this model, it is assumed that the chemical potential shifts toward the band edge and the light and heavy valence bands move close to each other with increasing In_2Te_3 concentration. First principles calculations should be a powerful method to verify the origin of the enhanced density of states that must accompany the increasing Seebeck coefficient as the concentration of In_2Te_3 increases. In addition, the rising resistivity leads to lower electronic thermal conductivity and the lattice thermal conductivity is also reduced due to strong phonon scattering by alloying disorder and vacancies. As a result, *ZT* is enhanced to 1.35 at 823 K for x = 0.05, a value comparable to the best modified TAGS materials. According to Narducci's suggestion[28], high power factor TE materials are more favorable for large-scale power generation. Therefore, these materials, which possess much higher power factors than TAGS materials and other TE tellurides, are very appealing candidates for practical applications.

Acknowledgements

This work is supported as part of the Center for Revolutionary Materials for Solid State

Physical Chemistry Chemical Physics Accepted Manuscript

Energy Conversion, an Energy Frontier Research Center funded by the US Department of Energy, Office of Science, Office of Basic Energy Sciences under Award Number DE-SC0001054.

References

1. J. P. Heremans, M. S. Dresselhaus, L. E. Bell and D. T. Morelli, *Nat. Nanotechnol.*, 2013, **8**, 471-473.
2. A. F. Ioffe, *Semiconductor Thermoelements, and Thermoelectric Cooling*, Infosearch, 1957.
3. Y. Z. Pei, X. Y. Shi, A. LaLonde, H. Wang, L. D. Chen and G. J. Snyder, *Nature*, 2011, **473**, 66-69.
4. Q. Zhang, B. L. Liao, Y. C. Lan, K. Lukas, W. S. Liu, K. Esfarjani, C. Opeil, D. Broido, G. Chen and Z. F. Ren, *P. Natl. Acad. Sci. USA*, 2013, **110**, 13261-13266.
5. L. D. Zhao, H. J. Wu, S. Q. Hao, C. I. Wu, X. Y. Zhou, K. Biswas, J. Q. He, T. P. Hogan, C. Uher, C. Wolverton, V. P. Dravid and M. G. Kanatzidis, *Energ. Environ. Sci.*, 2013, **6**, 3346-3355.
6. E. M. Levin, M. F. Besser and R. Hanus, *J. Appl. Phys.*, 2013, **114**, 083713.
7. N. V. Kolomoets, E. Y. Lev and L. M. Sysoeva, *Sov. Phys. Solid State*, 1964, **6**, 551-556.
8. Y. Gelbstein, J. Davidow, S. N. Girard, D. Y. Chung and M. G. Kanatzidis, *Adv. Energy Mater.*, 2013, **3**, 815-820.
9. A. H. Edwards, A. C. Pineda, P. A. Schultz, M. G. Martin, A. P. Thompson, H. P. Hjalmarson and C. J. Umrigar, *Phys. Rev. B*, 2006, **73**, 045210.
10. K. M. Rabe and J. D. Joannopoulos, *Phys. Rev. B*, 1987, **36**, 3319-3324.
11. E. A. Skrabek and D. S. Trimmer, in *CRC Handbook of Thermoelectrics*, ed. D. M. Rowe, CRC Press, Boca Raton, FL, 1995, p. 267.
12. J. R. Salvador, J. Yang, X. Shi, H. Wang and A. A. Wereszczak, *J. Solid State Chem.*, 2009, **182**, 2088-2095.
13. S. H. Yang, T. J. Zhu, T. Sun, S. N. Zhang, X. B. Zhao and J. He, *Nanotechnology*, 2008, **19**, 245707.
14. F. Fahrnbauer, P. Urban, S. Welzmiller, T. Schröder, T. Rosenthal and O. Oeckler, *Journal of Solid State Chemistry*, 2013, **208**, 20-26.
15. T. Rosenthal, M. N. Schneider, C. Stiewe, M. Döblinger and O. Oeckler, *Chemistry of Materials*, 2011, **23**, 4349-4356.
16. T. Rosenthal, S. Welzmiller and O. Oeckler, *Solid State Sciences*, 2013, **25**, 118-123.
17. T. Schröder, S. Schwarzmüller, C. Stiewe, J. de Boor, M. Hölzel and O. Oeckler, *Inorganic Chemistry*, 2013, **52**, 11288-11294.
18. J. F. Deng, J. Q. Li, R. F. Ye, X. Y. Liu, F. S. Liu and W. Q. Ao, *Journal of Alloys and Compounds*, 2014, **585**, 173-177.
19. L. Weintraub, J. Davidow, J. Tunbridge, R. Dixon, M. J. Reece, H. Ning, I. Agote and Y. Gelbstein, *Journal of Nanomaterials*, 2014, **2014**, 7.
20. E. I. Rogacheva, N. M. Pansenko and A. I. Melikhova, *Inorg. Mater.*, 1974, **10**, 1544-1547.

Physical Chemistry Chemical Physics Accepted Manuscript

21. Y. Z. Pei and D. T. Morelli, *Appl. Phys. Lett.*, 2009, **94**, 122112.
22. B. A. Cook, M. J. Kramer, X. Wei, J. L. Harringa and E. M. Levin, *J. Appl. Phys.*, 2007, **101**, 053715.
23. J. E. Lewis, *Phys. Status Solidi B*, 1973, **59**, 367-377.
24. M. Baleva, *Phys. Status Solidi B*, 1980, **99**, 341-346.
25. Y. W. Tung and M. L. Cohen, *Phys. Rev.*, 1969, **180**, 823-826.
26. Y. Gelbstein, B. Dado, O. Ben-Yehuda, Y. Sadia, Z. Dashevsky and M. P. Dariel, *J. Electron. Mater.*, 2010, **39**, 2049-2052.
27. T. Rosenthal, S. Welzmiller and O. Oeckler, *Solid State Sci.*, 2013, **25**, 118-123.
28. D. Narducci, *Appl. Phys. Lett.*, 2011, **99**, 102104.

Figure and Table Captions

Figure 1. (a) XRD patterns for hot-pressed $(In_2Te_3)_x(GeTe)_{3-3x}$ samples, and (b) specific heat capacity as a function of temperature for all samples. The inset in (a) is a magnification of the patterns between $41^o \leq 2\theta \leq 45^o$. Note that large peaks in (b) are associated with the rhombohedral to cubic phase transition and the peak temperature monotonically decreases with increasing x.

Figure 2. Electrical transport properties as a function of temperature for $(In_2Te_3)_x(GeTe)_{3-3x}$ samples. (a) electrical resistivity; (b) Seebeck coefficient; (c) Hall coefficient and Seebeck coefficient for all samples from 100 to 300 K. Open symbols are for Seebeck coefficient and closed ones are for Hall coefficient. Solid and dashed lines are fitting results using a two-band model for the Seebeck coefficient and the Hall coefficient, respectively. (d) power factor.

Figure 3. Mobility data for $(In_2Te_3)_x(GeTe)_{3-3x}$ in the temperature range of 2 K – 300 K.

Physical Chemistry Chemical Physics Accepted Manuscript

Figure 4. (a) Thermal conductivity and (b) lattice thermal conductivity as a function of temperature for $(In_2Te_3)_x(GeTe)_{3-3x}$ samples. The inset in (b) is the calculated temperature dependent Lorenz number for all samples.

Figure 5. *ZT* as a function of temperature for $(In_2Te_3)_x(GeTe)_{3-3x}$ samples.

Table 1. Hole concentration and mobility for $(In_2Te_3)_x(GeTe)_{3-3x}$ samples at 200 K and 300 K respectively extracted from measurements of the Hal effect and electrical resistivity. Note that the data are not available for the x = 0.20 sample at 300 K due to the nonlinear behavior of the Hall resistance as a function of the magnetic field.

Table 2. The chemical potential E_l relative to the light VBM, energy separation ΔE between the light and the heavy VBM, the temperature coefficients of E_l and ΔE, and the Lorenz number for $(In_2Te_3)_x(GeTe)_{3-3x}$ samples at 300 K.

Physical Chemistry Chemical Physics Accepted Manuscript

Figure 1(a)

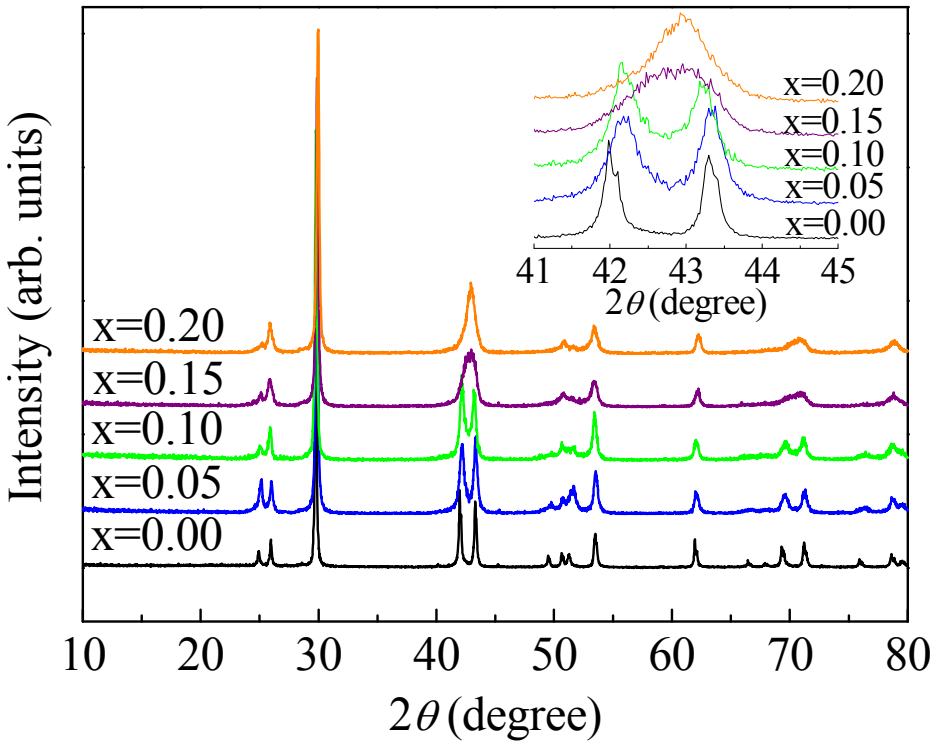

Physical Chemistry Chemical Physics Accepted Manuscript

Figure 1(b)

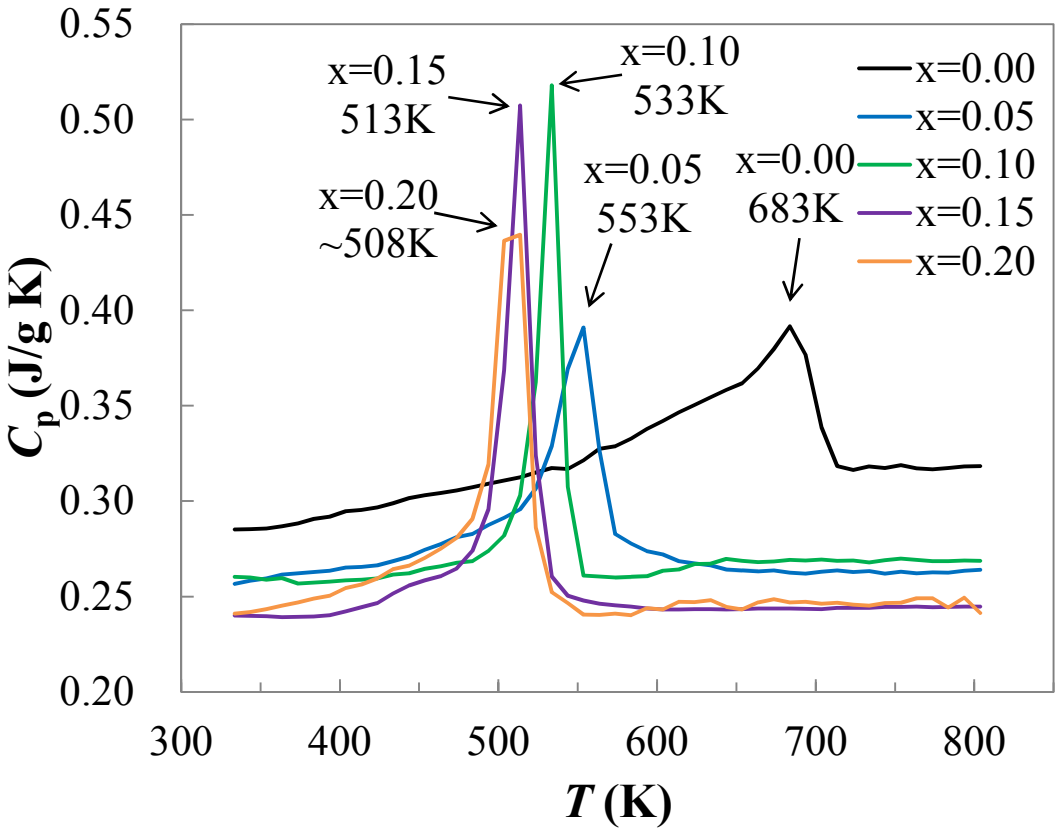

Physical Chemistry Chemical Physics Accepted Manuscript

Figure 2

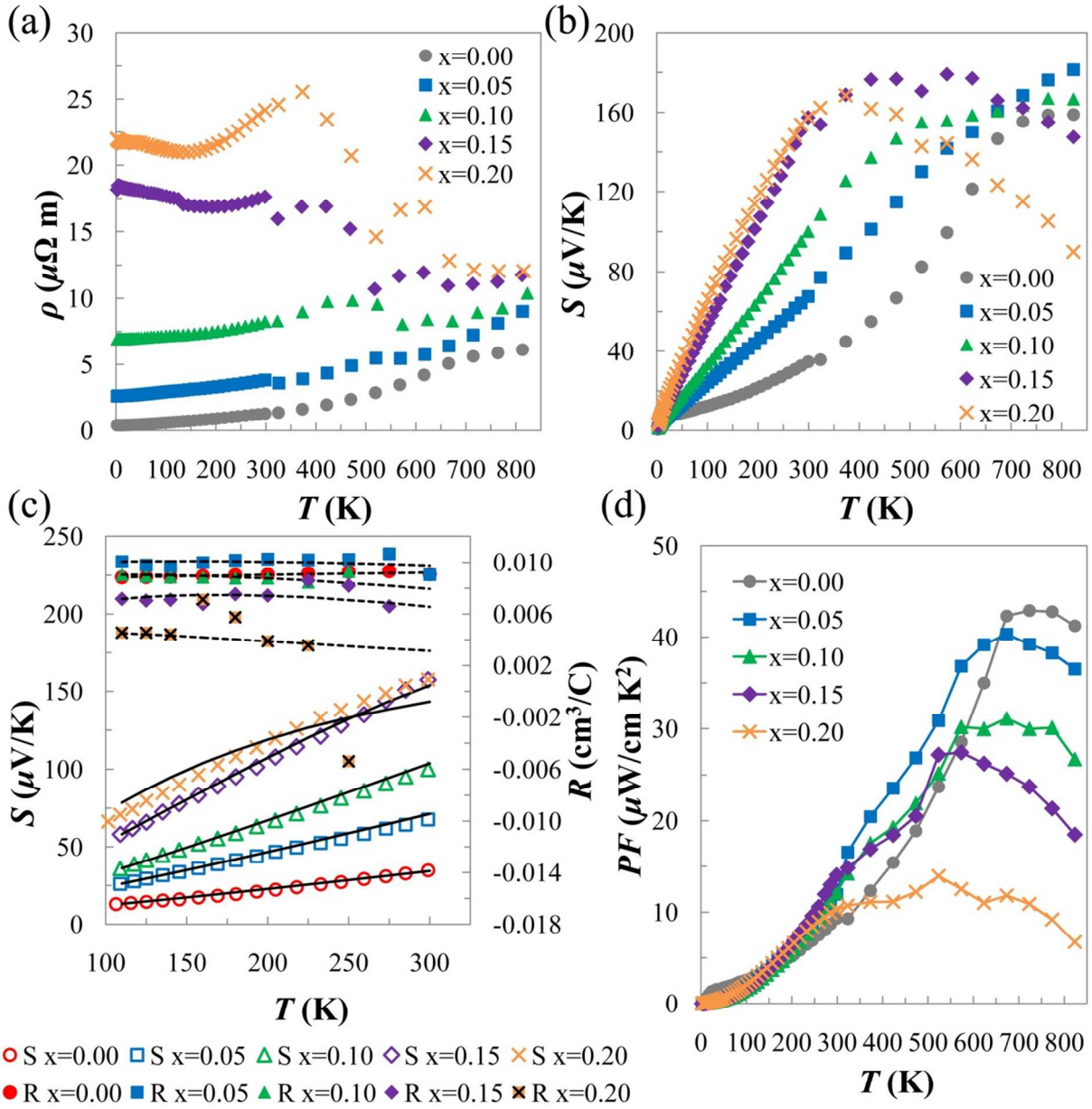

Physical Chemistry Chemical Physics Accepted Manuscript

Figure 3

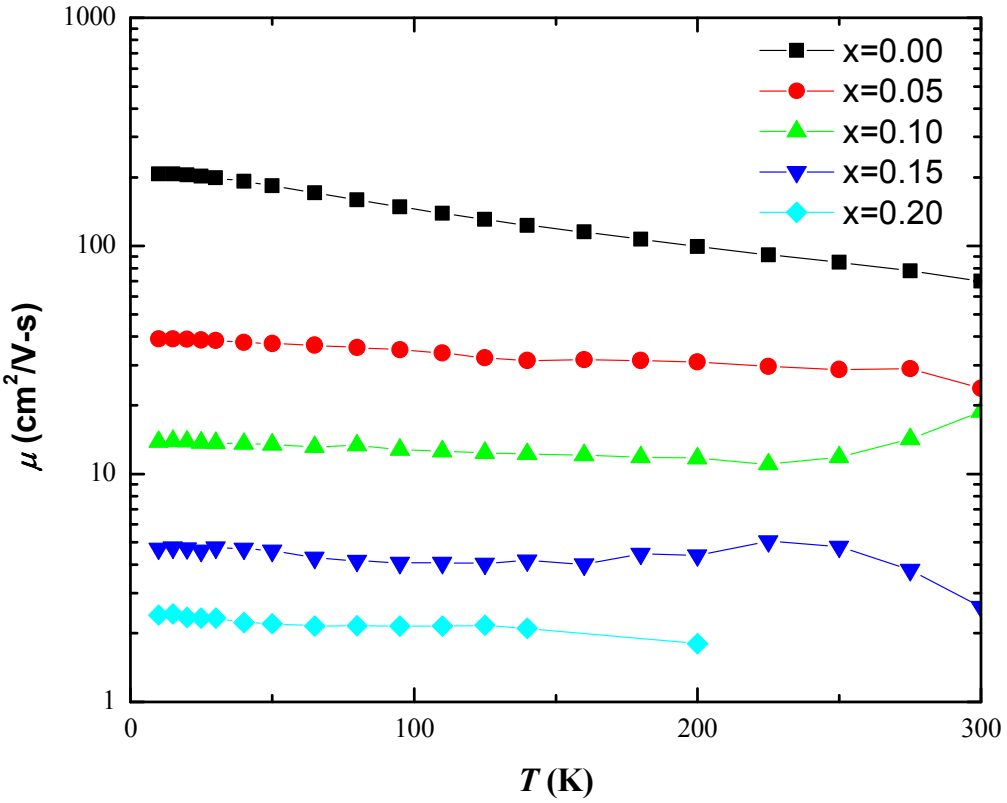

Physical Chemistry Chemical Physics Accepted Manuscript

Figure 4

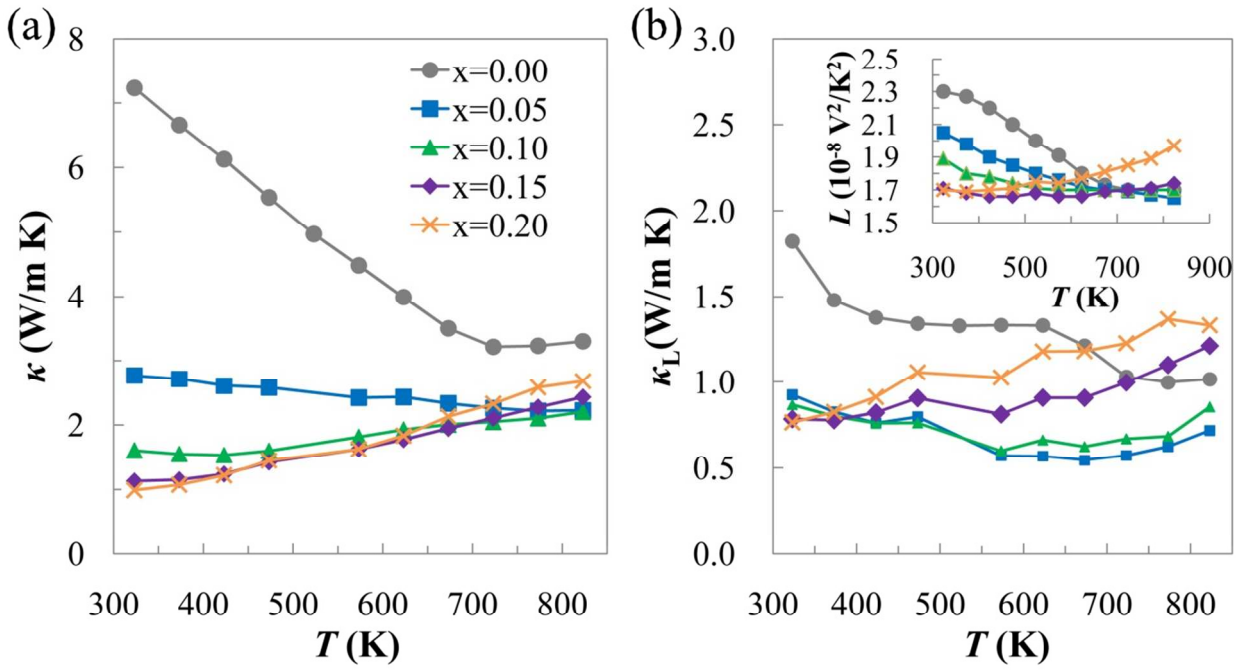

Physical Chemistry Chemical Physics Accepted Manuscript

Figure 5

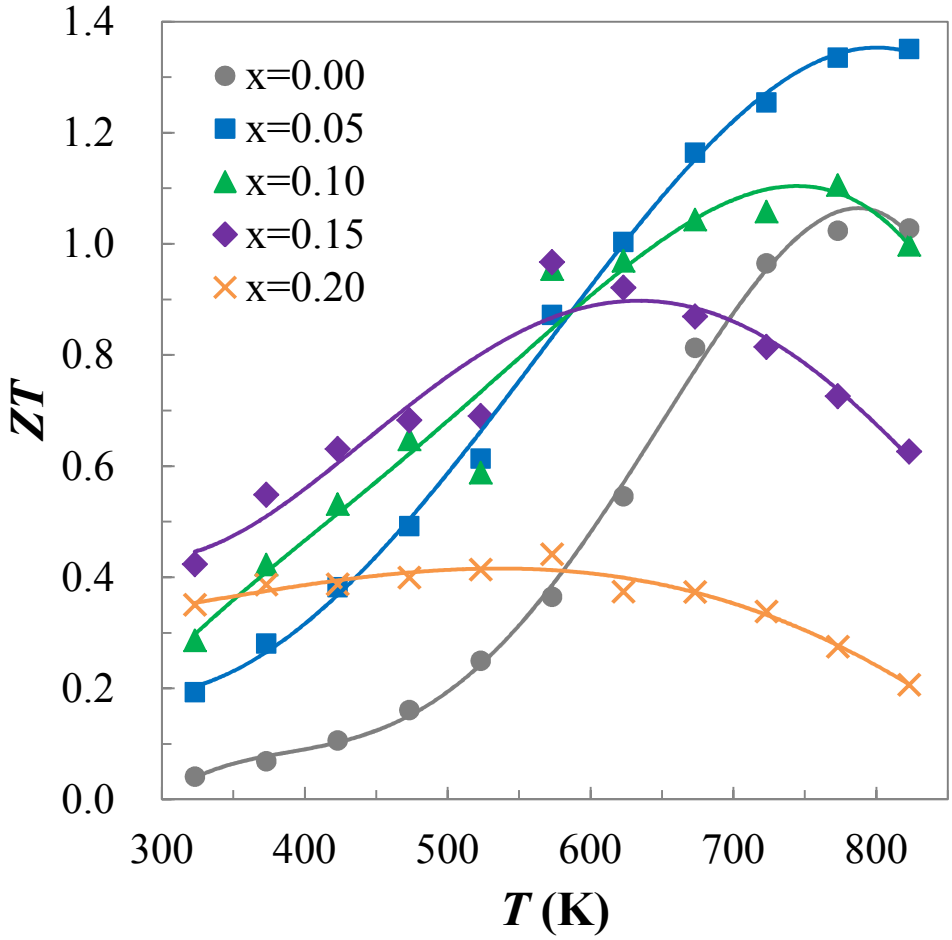

Physical Chemistry Chemical Physics Accepted Manuscript

Table 1

Sample	x=0.00	x=0.05	x=0.10	x=0.15	x=0.20
p_H (10^{20} cm^{-3}) 200 K / 300 K	6.9 / 6.9	6.1 / 6.9	7.1 / 4.0	8.4 / 13.7	16.1 / -
μ_H (cm^2 $V^{-1}s^{-1}$) 200 K / 300 K	98 / 70	31 / 24	12 / 19	4.4 / 2.6	1.8 / -

Table 2

Sample	E_l (eV)	ΔE (eV)	dE_l/dT (10^{-4} eV/K)	$d\Delta E/dT$ (10^{-4} eV/K)	L (10^{-8} V^2/K^2)
x=0.00	0.22	0.36	-0.4	5.3	2.33
x=0.05	0.18	0.22	-0.7	0.8	2.20
x=0.10	0.15	0.16	-1.9	-1.2	2.02
x=0.15	0.07	0.06	-2.5	-1.6	1.74
x=0.20	0.002	-0.03	0	0.07	1.75

Physical Chemistry Chemical Physics Accepted Manuscript